PAPER

Long-working-distance microscopic imaging through a scattering medium using supercontinuum illumination

IOP Publishing Physica Scripta
Phys. Scr. 94 (2019) 045505 (6pp) https://doi.org/10.1088/1402-4896/aafdc3

Long-working-distance microscopic imaging through a scattering medium using supercontinuum illumination

Zhe Zhao, Wenjiang Tan, Yipeng Zheng, Mingxin Wang and Xiaojing Liu

Key Laboratory for Physical Electronics and Devices of the Ministry of Education & Shaanxi Key Lab of Information Photonic Technique, School of Electronics & information Engineering, Xi'an Jiaotong University, Xianning-xilu 28, Xi'an, 710049, People's Republic of China

E-mail: tanwenjiang@mail.xjtu.edu.cn

Received 6 August 2018, revised 27 December 2018
Accepted for publication 11 January 2019
Published 31 January 2019

Abstract

We demonstrate long-working-distance microscopic imaging through scattering media, in which a homemade long-working-distance microscopic imaging unit is used to increase the spatial frequency and a femtosecond-laser-induced supercontinuum is used to suppress the harmful speckles to improve object visibility. Although the aim of the imaging system is to study the real fuel spray, the presented work is mainly to focus on the performance of this long-working-distance microscopic imaging system. The results shows that the working distance and the maximum spatial resolution of our imaging system could reach up to 20 cm and 3.5 μm, respectively. Even when the optical depth of the scattering media reaches approximately 12, the maximum spatial resolution could be maintained at 3.8 μm. Compared with some previous imaging systems for fuel spray diagnostics, our long-working-distance microscopic imaging system shows the best overall performance and offers a good candidate for imaging the microscopic structures of fuel sprays.

Keywords: scattering, spray diagnostic, long-working-distance microscopic, supercontinuum

(Some figures may appear in colour only in the online journal)

1. Introduction

Rapid liquid breakup and fast atomization occur in the near-nozzle exit under high pressure and high temperature conditions in a diesel engine [1]. The major steps of the combustion process are the injection and mixing of fuel to create an efficient gas-phase reaction. A large number of micro-droplets, liquid cores, and cavitation at high velocities exist in the liquid jet fuel spray, which is in a strong scattering environment with turbulence and cavitation in the near-nozzle region. The complex dynamics of internal flow occurring in the dense spray region would be obscured by intense scattering photons originating from the dense droplet cloud when conventional optical diagnostic techniques are used, such as Raman spectroscopy, laser-induced fluorescence, and laser Doppler velocimetry [2–4]. A great amount of effort has been devoted to the development of advanced optical techniques for diagnosing fuel sprays [5–9].

In these diagnostic techniques, lasers are widely used as light sources owing to their prominent photon degeneracy. For example, ultrafast time-gated ballistic imaging has been used for different kinds of sprays to image the liquid/gas interfaces of intact liquid structures inside the dense regions [10]. However, interference among the scattered laser photons causes speckles in the imaging results. These speckles severely degrade the image quality and hinder object discrimination [11]. Some efforts have recently been made to suppress the speckles using incoherent light sources. Cao *et al* demonstrated that random lasers with low spatial coherences could clearly recognize objects hidden under intense optical scattering conditions via speckle-free full-field imaging [12]. Some traditional incoherent light sources, such as thermal sources and light emitting diodes, can also provide speckle-free full-field imaging. Unfortunately, these illumination sources avoid speckles but lack sufficient power per mode

and spectral control for applications requiring high-speed imaging or imaging in absorbing or scattering media [13–15]. Low-spatial-coherence electrically pumped semiconductor lasers generate lower spatial coherences and maintain higher powers per mode compared to traditional incoherent light sources. However, the required optical pumping, along with the large size and cost of these systems, may limit their use outside of a research setting [16]. In the last two decades, femtosecond lasers have been reported as a promising tool for laser processing and ultrafast measurements [17–19]. Our previous work indicates that the supercontinuum (SC) induced by femtosecond laser can also be used to suppress the speckle due to its degeneration of coherence [20]. Besides, the SC is very suitable for imaging rapidly changing object without motion blurring effects owing to its short pulse duration compared with the incoherent light sources mentioned above.

However, our previous imaging system using SC can only be used to resolve macroscopic object greater than tens of micrometers, similar to most of the optical imaging systems diagnosing the near-nozzle regions of the fuel sprays [21]. But the information obtained from the microscopic development of the spray, such as the liquid-gas interface, ligament size, voids, and liquid cores in the near-nozzle region, is of great importance in understanding the atomization and combustion process; it is thus necessary to develop some microscopic imaging technique for diagnosing fuel sprays. Moreover, the near-zone region of a fuel spray has high temperature and pressure, which requires an imaging system with a long-working distance of tens of centimeters to avoid contamination or damage to the optical elements [22]. However, the microscopic components of most current optical microscopic imaging systems are generally commercial microscopic imaging units with relatively short working distances of several centimeters.

In this study, we improve our previous SC-illumination imaging system and demonstrate long-working-distance microscopic imaging through scattering media, in which a femtosecond laser-induced SC is used to suppress the harmful speckles to improve object visibility and a homemade long-working-distance microscopic imaging unit is used to improve the spatial frequency. The results show the working distance and the maximum spatial frequency of our imaging system could reach up to 20 cm and 144 lp mm^{-1}, respectively. Even when the optical depth (OD) of the scattering media reaches about 12, the image remained identifiable and the maximum spatial frequency could be maintained at 131 lp mm^{-1}. As the OD of the near field of a diesel spray is on the order of 8–10 [21], our long-working-distance microscopic imaging system offers a good candidate for imaging the microscopic structures of the fuel sprays.

2. Experiments

The experimental optical setup is shown in the figure 1. A Ti: sapphire laser system (Libra-USP-HE, Coherent Inc., USA) produces the femtosecond laser pulse, which has a pulse

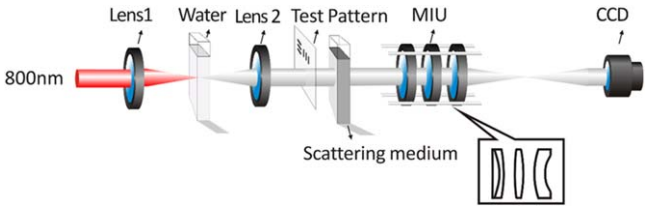

Figure 1. Long-working-distance microscopic imaging setup through scattering medium using supercontinuum illumination. MIU: the long-working-distance microscopic imaging unit.

width of 50 fs, a center wavelength of 800 nm, and an energy of 3.5 mJ per pulse at a repetition frequency of 1 kHz. The ultrafast laser is then introduced to lens L1 with a focal length of $f1 = 150$ mm and focused into a 4 cm thick quartz cuvette filled with distilled water to generate the SC as the light source. As the stability of SC is dependent on the power and the spatial distribution of incident light, the pulse energy of incident femtosecond fundamental frequency (FF) laser is adjusted to be less than 1 mJ and the spot size of the incident laser is also carefully adjusted to ensure the stability of SC. Besides, the pulse width of the femtosecond laser is also expanded to be less than 200 fs before lens L1 due to the dispersion of the optical elements located between the laser source and the imaging system. Then, a Lens (L2) with a focal length of $f2 = 100$ mm is used to collect the divergent SC to generate parallel light. A 1951 USAF resolution test chart is placed as the imaged target on the object plane before the optically-dense media, which is composed of a suspension of 3.13 μm diameter polystyrene spheres in a cubic cell. We obtain different images using five kinds of ODs of the samples. The OD, defined as $OD = -\ln(I/I_0)$, was measured with the OKG method [23]. Here, I and I_0 were the light intensities exiting and entering the scattering media. The modulated light of the test pattern was transmitted through 200 mm and is introduced into a homemade long-working-distance microscopic imaging unit. The details are shown in following section. The long-working-distance microscopic imaging unit is mounted on a cage that allows it to be accurately adjusted. The shadowgraphs are recorded by a monochrome charge-coupled device (CCD) camera (INFINITY3-1M-NS-TPM, Lumenera Corporation, Canada). The quantum efficiencies of our monochrome CCD camera are higher than 10% operating at wavelengths ranging from 400 to 850 nm. Its highest quantum efficiency is about 60% at 500 nm. Although the aim of our imaging system is to study the real fuel spray, the presented work is mainly to focus on the performance of this long-working-distance microscopic imaging system. As a result, the 1951 USAF resolution test chart is used to replace the spray as the test sample.

As the spectral characteristic of the light source is important for performance of the imaging systems, the chirp characteristic of the SC is measured by using an optical Kerr gated method [19], as shown in figure 2. The spectra of the SC and the FF laser are shown in the inset of the figure 2. From figure 2, we can see that the pulse width of the SC is about 14 ps and the spectrum of the SC ranges from about 400 to 850 nm. Moreover, the spectral intensity of the SC

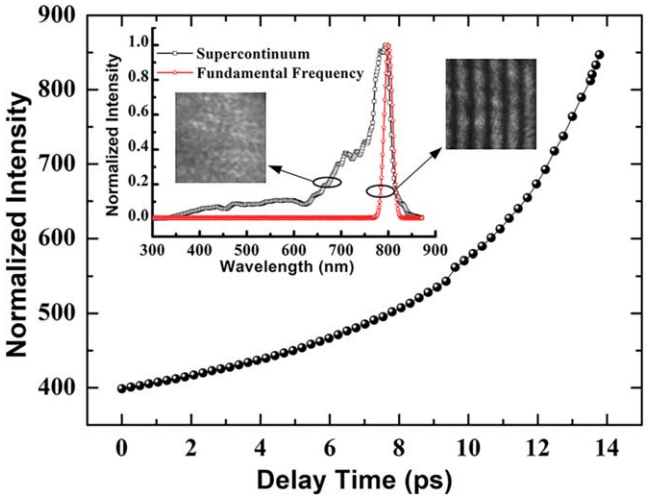

Figure 2. Characteristics of the supercontinuum and the fundamental frequency laser.

rapidly decreases as its wavelength diverges from the fundamental wavelength. Because the coherence length is inversely proportional to the bandwidth of the light source, we could infer that the SC has a low coherence compared with the FF laser. A homebuilt Michelson interferometer is further used to estimate the coherence of the SC and the FF laser, respectively. As shown in the inset of the figure 2, we can see that the interference pattern of the SC is invisible but clearly visible for the FF laser, which confirms the degeneration of coherence of the SC. In addition, it should be noted that although increasing the incident fundamental laser power density inside of the water in our experiment, for example using a shorter focus lens, might increase the SC pulse energy and broad the SC spectral range to a certain extent. The improvement of the SC pulse energy will be restricted because the incident fundamental laser pulse intensity should be less than the damage threshold of the water. And the broadening wavelength range will be ultimately determined by the photon energy of the incident laser and the band-gap energy of the water. It might be helpful to improve the SC pulse energy by using a micro-lens array to focus the fundamental laser into the other transparent condensed media with larger band-gap energy.

3. Designing of microscopic imaging unit

As mentioned above, due to the long-working distance requirement, we have designed a long-working-distance microscopic imaging unit with a working distance of 200 mm. The microscopic imaging unit has three basic components: an achromatic doublet, a convex lens, and a meniscus lens. All the surfaces of the lenses are spherical. The simulation uses the wavelength of 750–850 nm which is the main distribution of SC in intensity as shown in figure 2. The imaging quality of the system can effectively improve by the rational design of material, curvature radius, focal length. K9 glass is the primary material. Because the aberration is smaller with the decreasing sum of the curvature radii, a ZF6 material lens with a large refractive index is used to reduce the sum of the curvature radii. The sum of the focal lengths approaches zero for the designed microscopic imaging unit. The structure enables a large field of view of 800 μm with an NA of 0.1.

Figure 3(a) shows the predicted geometric spot size is smaller than the Airy disk. As shown in figure 3(b), the predicted modulation transfer function (MTF) of the homemade unit. The MTFs of the meridional and sagittal directions of each field are all overlapping with the diffraction limited MTF. All these figures indicate that the aberrations, such as the spherical aberration, coma aberration, and field curvature, are well corrected for. The optical layout and the finished product of the fabricated and assembled unit are shown in figures 3(c) and (d). The basic parameters of the long-working-distance microscopic imaging unit are listed in table 1. These lenses are mounted inside a cage system, which provides a rigid construction. Then the long-working-distance microscopic imaging unit is used in the experimental setup shown in figure 1.

4. Results and discussion

In the imaging experiment, we firstly obtain a direct image at OD = 0 using the imaging system of SC illumination shown in figure 1 without the scattering medium to qualitatively evaluate the performance of the long-working-distance microscopic imaging system. The result is shown in figure 4(a), in which the image is flat-field, visible, and highly identifiable. Then, we obtain some images at different ODs. For a comparison, images using FF laser illumination are also obtained as shown in figure 4(b), when the optical imaging system has no quartz cuvette placed in the back-focal-plane of lens L1. The images obtained with the long-working-distance microscopic imaging system using SC illumination are shown in figure 4(c). The images in figure 4(b) are filled with speckles, which result in intense noise and considerably obscure the patterns on the resolution test chart. The corruption worsens, reaching a disastrous level with the OD increasing from 10 to 14. As shown in figure 4(c), the images are clear and visible in a strong scattering environment due to the speckle suppression using SC illumination. Even at the OD of 14, most of bars in the image are still identifiable. In other words, the long-working-distance microscopic imaging system using SC illumination provides good image quality and improves the contrast and visibility of the images, which allows better identification.

Moreover, we calculate the contrast-to-noise ratio (CNR) at different ODs to quantitatively analyze the images in figure 5. The CNR is used to describe the identification of the object against a given background, defined as $(I_A - I_B)/((\sigma_A + \sigma_B)/2)$. I is the intensity of the signal-producing structures. A and B are, respectively, the bar and its surrounding background in the resolution test chart. σ refers to the standard deviation of the pixel intensity. As shown in figure 5, the CNR curve measured without scattering is high and the maximum CNR reaches up to 5 at the spatial

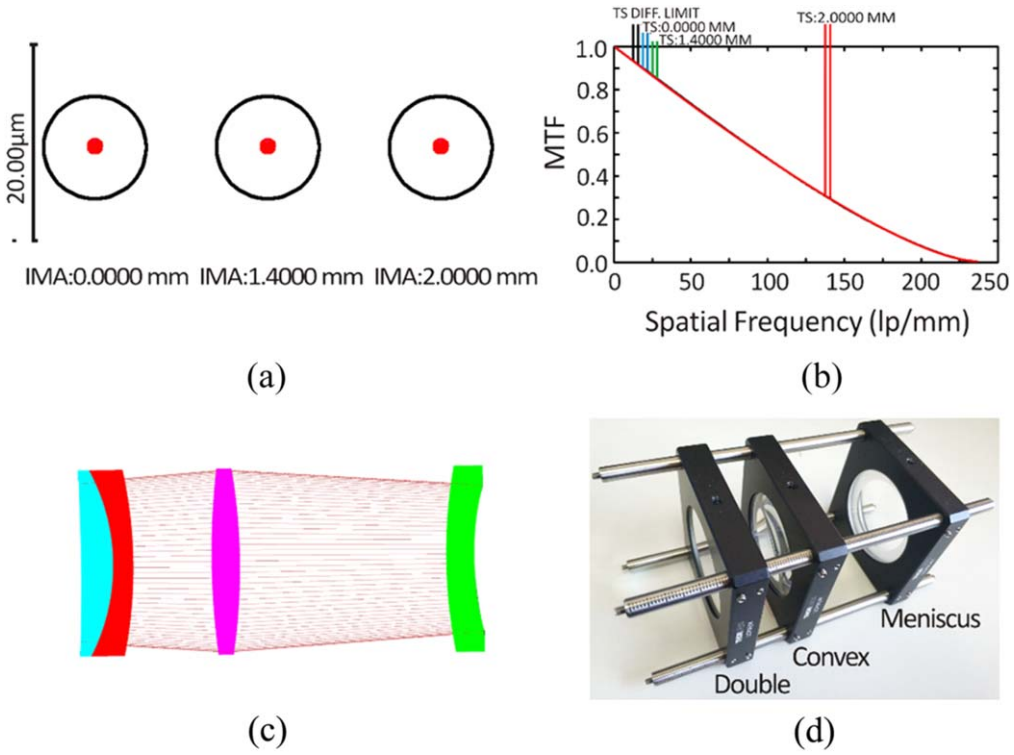

Figure 3. Long-working-distance microscopic imaging unit. (a) Geometric spot diagram for three different field positions. The black circles are the Airy disks. (b) Modulation transfer function. (c) Optical layout. (d) The photograph. MTF: modulation transfer function.

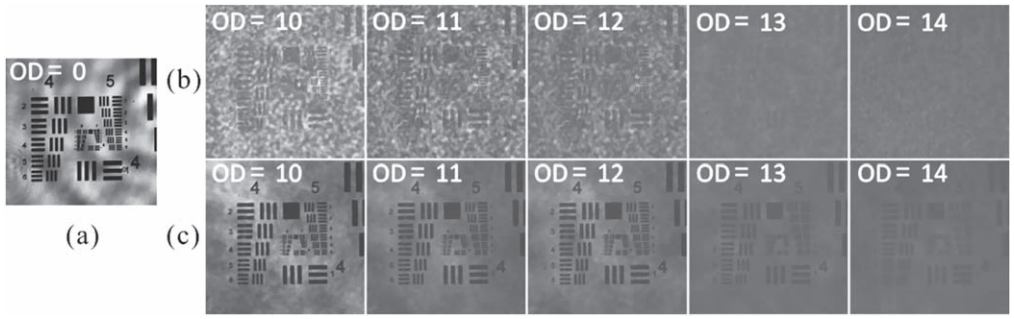

Figure 4. (a) Direct image obtained using the long-working-distance microscopic imaging system using supercontinuum illumination. The images obtained using (b) fundamental frequency laser and (c) supercontinuum illumination at different ODs, based on the long-working-distance microscopic imaging unit, are also shown. OD: optical depth.

Table 1. Parameters of the long-working-distance microscopic imaging unit. $R1$, $R2$ and $R3$ are the radius of curvature of each surface of the lens.

Lens type	$R1$ (mm)	$R2$ (mm)	$R3$ (mm)	Focus (mm)	Diameter (mm)	Glass material
Double	−576	−50	−112	182/484	50.8	K9/ZF6
Convex	−186	−147	/	161	50.8	K9
Meniscus	124	74	/	−382	50.8	K9

frequency of 16 lp mm^{-1}. The maximum starting value begins at 2 for the CNR curves obtained using FF laser illumination and these CNR curves quickly drop below 1 with increasing spatial frequency. By contrast, in the strong scattering environment with ODs of 10–12, the CNR curves obtained using SC illumination all have a starting value of approximately 4 and slowly decrease with increasing spatial frequency. Increasing the OD to 14, the CNR curve obtained using SC illumination still has a starting value of up to 3. Compared with the images obtained using FF laser illumination at the same OD, the images obtained using SC illuminating have higher CNRs.

In terms of the definition of the CNR, the characters would not be identifiable at all when the CNR is less than 1. Specifically, the spatial frequency of the images at CNR = 1 is equivalent to the maximum spatial frequency of the images

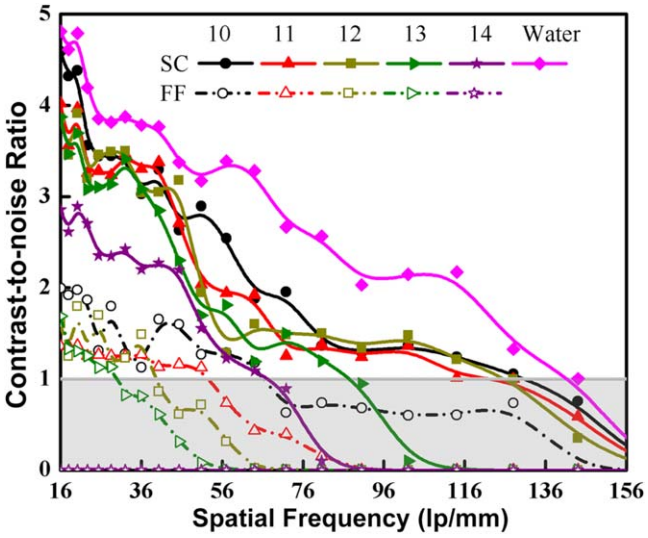

Figure 5. Contrast-to-noise ratio versus spatial frequency for images obtained by the long-working-distance microscopic imaging system using SC illumination (solid) and fundamental frequency laser illumination (dotted). The gray background indicates the CNR < 1 where the imaging objects would not be identifiable. lp/mm: line pairs/mm; SC: supercontinuum; FF: fundamental frequency laser.

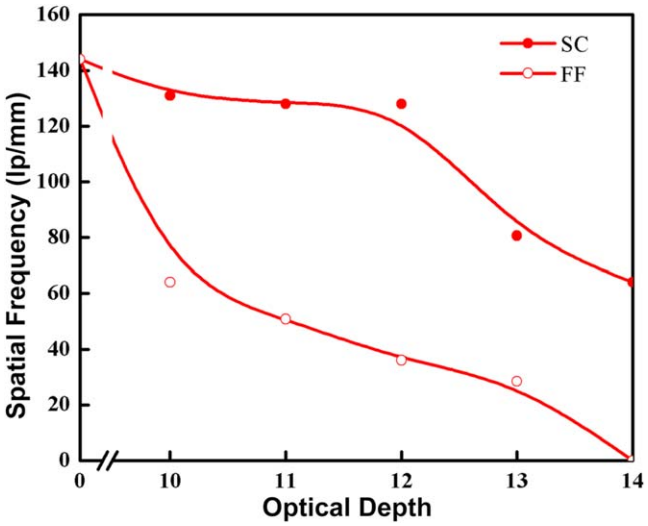

Figure 6. Maximum spatial frequency versus optical depth for images obtained by the long-working-distance microscopic imaging system using SC illumination (solid) and fundamental frequency laser illumination (hollow). lp/mm: line pairs/mm; SC: supercontinuum; FF: fundamental frequency laser.

under the current conditions. We further draw the curves of the maximum spatial frequency versus OD shown in figure 5. And as the OD increases, the maximum spatial frequency decreases in figure 5. The maximum spatial frequency of the image is 144 lp mm^{-1}, corresponding to the spatial resolution of 3.5 μm at OD $= 0$. The curve with hollow circles in figure 6 shows that the maximum spatial frequencies of the images obtained using FF laser illuminating are 64 lp mm^{-1} (7.8 μm), 50.8 lp mm^{-1} (9.8 μm), 36 lp mm^{-1} (13.9 μm), and 28.5 lp mm^{-1} (17.5 μm) at OD $= 10$, 11, 12, and 13, respectively. The maximum spatial frequencies quickly drop to 0 as the OD increases to 14. Compared to the images obtained using the FF laser illumination, the images obtained using SC illumination can realize a higher maximum spatial frequency in strong scattering conditions. The maximum spatial frequency can reach up to 131 lp mm^{-1} (3.8 μm) when OD $\leqslant 12$, which is slightly less than the maximum spatial frequency at OD $= 0$, due to the multiple scattering photons. The maximum spatial frequency slowly decreases to 80.6 lp mm^{-1} (6.2 μm) at OD $= 13$. Even when the OD increases to 14, the maximum spatial frequency still remained at 64 lp mm^{-1} (7.8 μm). Overall, at a high OD of 12, the long-working-distance microscopic imaging system using SC illumination in the case of a long working distance of 200 mm can realize simultaneously a flat-field and distinguishable image and the maximum spatial frequency of 131 lp mm^{-1}, corresponding to the spatial resolution of 3.8 μm.

Table 2. Comparison of the working distance, optical depth and image resolution obtained in this paper with those reported in earlier literature. OKG system: optical Kerr gated ballistic imaging system. LWDM: long-working-distance microscopy.

Optical configuration	Working distance (cm)	Optical depth	Resolution (μm)
Ultrafast high-repetition imaging system [24]	38	0	15.5
		10	/
4f OKG system [25]	25	0	13
		10	28.2
4f OKG system [5]	15	0	12.8
		12	23.8
4f OKG system [26]	20	0	10.3
		10	/
2f OKG system [25]	22.5	0	8.5
		10	25.6
LWDM OKG system [27]	24.5	0	/
		5.2	7
Our imaging system	20	0	3.5
		12	3.8

Further, we compare the working distance, optical depth and imaging resolution of our imaging system with some previous imaging systems for fuel spray diagnostics [5, 24–27] as shown in table 2. From table 2, we can see that the working distances of these non-microscopic imaging systems were tens of centimeters to avoid contamination or damage to the optical elements. However, their spatial resolutions are larger than 10 μm for non-scattering conditions and deteriorated more than one time for scattering conditions with ODs being about 10. Although a higher spatial resolution of about 7 μm with a working distance of 24.5 cm has been performed in a long-working-distance microscopic OKG system, the OD was about 5.2. Compared with those imaging systems described above, our imaging system has a highest spatial resolution of about 3.5 μm with a working distance of 20 cm in a non-scattering environment. Even when the OD of the scattering media

increased to about 12, the spatial resolution of our imaging system could maintain at 3.8 μm. The results show that our imaging system has the best overall performance and is suitable for imaging the microscopic structures of intense scattering fuel sprays.

5. Conclusion

We demonstrate long-working-distance microscopic imaging through scattering media, in which a homebuilt long-working-distance microscopic imaging unit and a femtosecond-laser-induced SC are used in order to improve the spatial frequency and suppress the harmful speckles for improving object visibility. The imaging system is able to achieve flat-field imaging. The results show that the working distance and maximum spatial frequency of our imaging system could reach up to 20 cm and 144 lp mm^{-1}, respectively, corresponding to the spatial resolution of 3.5 μm. Even when the OD of the scattering media reached ~12, the image remained identifiable and the maximum spatial resolution could be maintained at 3.8 μm. Moreover, the maximum spatial resolution reaches 7.8 μm at OD = 14. This long-working-distance microscopic imaging system offers a good candidate for imaging the microscopic structures of fuel sprays.

Acknowledgments

This work is supported by the National Natural Science Foundation of China (Grant Nos. 61690221, 61427816, 61205129), the Natural Science Basic Research Plan in Shaanxi Province of China (2018JM6012) and the Collaborative Innovation Center of Suzhou Nano Science and Technology.

ORCID iDs

Wenjiang Tan https://orcid.org/0000-0001-9822-0789

References

[1] Schmidt J B, Schaefer Z D, Meyer T R, Roy S, Danczyk S A and Gord J R 2009 *Appl. Opt.* **48** B137–44
[2] Rodrigues H C, Tummers M J, Veen E H V and Roekaerts D J E M 2015 *Combust. Flame* **162** 759
[3] Mulla I A, Dowlut A, Hussain T, Nikolaou Z M and Balachandran R 2016 *Combust. Flame* **165** 373
[4] Macphee A G, Tate M W P, CFY Y, Renzi M J and Ercan A 2002 *Science* **295** 1261–3
[5] Mathieu F, Reddemann M A, Palmer J and Kneer R 2014 *Opt. Express* **22** 7058
[6] Berrocal E, Kristensson E, Hottenbach P, Aldén M and Grünefeld G 2012 *Appl. Phys.* B **109** 683–94
[7] Idlahcen S, Rozé C, Méès L, Girasole T and Blaisot J B 2012 *Exp. Fluids* **52** 289–98
[8] Ramírez A I, Som S and Aggarwal S K 2009 *Exp. Fluids* **47** 119–34
[9] Wang L, Ho P P, Liu C, Zhang G and Alfano R R 1991 *Science* **253** 769–71
[10] Sedarsky D L, Paciaroni M E, Linne M A, Gord J R and Meyer T R 2006 *Opt. Lett.* **31** 906–8
[11] Shi Z, Zerom P and O Sullivan M N 2012 *Phys. Rev.* A **86** 3818–21
[12] Redding B, Choma M A and Cao H 2012 *Nat. Photon.* **6** 355–9
[13] Manin J, Bardi M, Pickett L M and Payri R 2016 *Int. J. Multiph. Flow* **83** 267–78
[14] Kuti O A 2013 *Fuel* **104** 838–46
[15] Karra P, Rogers T and Lappas P 2015 *SAE Technical Papers 2015* (https://doi.org/10.4271/2015-01-0002)
[16] Redding B, Cerjan A and Huang X 2015 *Proc. Natl Acad. Sci.* **112** 1304–9
[17] Nguyen V, Si J, Yan L and Hou X 2015 *Carbon* **95** 659–63
[18] Ma Y, Ren H and Si J 2012 *Appl. Surf. Sci.* **261** 722–6
[19] Tan W, Liu H, Si J and Hou X 2008 *Appl. Phys. Lett.* **93** 051109
[20] Zheng Y, Si J, Tan W, Ren Y H, Tong J and Hou X 2016 *Opt. Express* **24** 26338–43
[21] Linne M 2013 *Prog. Energy Combust.* **39** 403–40
[22] Sjoberg H, Manneberg G and Cronhjort A 1996 *Opt. Eng.* **35** 3591
[23] Tong J and Tan W 2011 *Opt. Eng.* **50** 43607
[24] Purwar H, Wang H and Tang M 2015 *Opt. Express* **23** 33396
[25] Rahm M, Paciaroni M, Wang Z, Sedarsky D and Linne M 2015 *Opt. Express* **23** 22444–62
[26] Idlahcen S, Mees L, Roze C, Girasole T and Blaisot J B 2009 *J. Opt. Soc. Am.* A **26** 1995
[27] Ren Y, Tan W, Zheng Y, Liu X and Tong J 2016 *Rev. Sci. Instrum.* **87** 63708